ELSEVIER

Biophysical Chemistry 79 (1999) 129–151

Biophysical Chemistry

Effective diffusion coefficients of K^+ and Cl^- ions in ion channel models

G.R. Smith, M.S.P. Sansom*

Laboratory of Molecular Biophysics, Rex Richards Building, Department of Biochemistry, University of Oxford, South Parks Road, Oxford OX1 3QU, UK

Received 23 November 1998; received in revised form 26 March 1999; accepted 27 March 1999

Abstract

We have used molecular dynamics simulations, corresponding to a total simulation time of 11 ns, to investigate the effective short-time local diffusion coefficient of potassium and chloride ions in a series of model ion channels. These models, which include channels formed by the fungal peptide alamethicin, by a synthetic leucine–serine peptide, and by the pore-lining M2 helix bundle of the nicotinic acetylcholine receptor, have a range of different secondary structures, diameters and hydrophobicities. We find that the diffusion coefficients of both ions are appreciably reduced in the narrower channels, the extent of the reduction being similar for both the anionic and cationic species. This suggests that a difference in mobility cannot be the source of the ion selectivity exhibited by some of the channels (for example, the leucine–serine peptide). We find no evidence for a reduction in mobility of either ion in the nAChR model. These results are broadly in line with a previous similar study of Na^+ ions, and may be useful in Poisson–Nernst–Planck, Eyring rate theory or Brownian dynamics calculations of channel conductance.

Keywords: Ion channel; Molecular dynamics simulation; Ionic diffusion coefficient; Potassium; Chloride; Conductance prediction

1. Introduction

Channels are integral membrane proteins that allow ions rapidly to cross the lipid bilayer, a process which otherwise has a timescale of days [1]. They are ubiquitous in both prokaryotic and eukaryotic cells and play vital roles in homeostasis, signaling (in electrically excitable tissues) and in producing and maintaining the membrane potential which is coupled to many other transport processes.

There is a great deal of functional information

* Corresponding author. Tel.: +44-1865-275-371; fax: +44-1865-275-182; e-mail: mark@biop.ox.ac.uk

0301-4622/99/$ - see front matter
PII: S0301-4622(99)00052-6

about ion channels, coming primarily from electrophysiology experiments: since the development of the patch-clamp technique, it has become possible to measure the current–voltage (I–V) relations of single channels as well as of whole cells, to investigate the time course of the channels' response to chemical and electrical stimulation, and to study the dependence of the I–V relations on the concentration and composition of the bathing electrolyte solutions and on point mutations in the channels [2]. Structural information is comparatively scarce. There are well-known difficulties in overexpressing and crystallizing membrane proteins for X-ray diffraction experiments, and their insolubility renders them unsuitable for solution NMR. Indeed, it is only recently that an X-ray structure has become available for a selective ion channel from one of the major families, the KcsA potassium channel of *Streptomyces lividans*, related to the voltage-gated potassium, sodium and calcium channels in eukaryotes [3]. The non-selective mechanosensitive channel MscL from *Mycobacterium tuberculosis* has also recently been solved [4]. Aside from these, atomic-resolution structural information is available only for model channels such as gramicidin A [5–8], porins [9,10], and the pore-forming toxin α-hemolysin [11]. For certain other channels lower-resolution information is available, for example for the nicotinic acetylcholine receptor [12,13] from cryo-EM studies, while for yet others, indirect evidence from mutagenesis experiments is the major source of information. Furthermore, even when an X-ray structure is available, it is sometimes unclear as to which functional state (e.g. open vs. closed) of the channel this represents.

To understand the connection between structure and function (i.e. to predict the I–V relation) should be easier for channels than for other membrane transport systems, because the transport process is passive, and the permeation pathway is relatively simple, an aqueous pore crossing the membrane; but it is nevertheless difficult to achieve quantitatively from first principles. If quantitative structure–function connections were possible, then the vast amount of physiological information that has been amassed would become much more valuable, because a putative channel structure that did not yield I–V relations in agreement with experiment could be rejected with confidence (even though the physiological data alone would probably be insufficient to determine the structure of the channel uniquely).

Why is the establishment of the structure–function connection so difficult? The systems are sufficiently complicated that numerical methods must be used, either for the numerical solution of the transport equations describing a simplified model or for the direct simulation of an atomistic model of the system. The two most commonly used simplified models are based either on the Nernst–Planck and Poisson equations [14,15] or the Eyring theory of kinetic transport over barriers. Both these approaches (the first in particular) can predict conductances in impressive agreement with experiment, but both contain free parameters which must be fitted, and which are problematic to interpret physically, so rendering them difficult to use predictively.

The most conceptually straightforward way of approaching the problem is probably via molecular dynamics (MD) simulation, where an atomistic model of the system is evolved in time by solving Newton's equations [16,17]. However, to extend the simulation time beyond approximately 10 ns is very major undertaking with presently-available computers; this is appreciably shorter than the typical timescale of physiological ion permeation ($\sim$ 100 ns–1 μs). A sensible 'hybrid' approach to adopt is therefore to use (relatively short) MD simulations to measure properties of the ion at a variety of different positions in the channel, and then to use these properties in a 'reduced model' of some kind [18–22]. The greatest success of this approach has probably been achieved in work on gramicidin [20,23–27]. In the work reported here we shall give results for local diffusion coefficients of K^+ and Cl^-, in various model ion channels, as part of a larger project which also involves the measurement of potentials of mean force and the development of methods to calculate conductance.

We have chosen to investigate a series of mod-

els which differ quite appreciably among themselves: some are helix bundles and one is a beta barrel, some are hydrophobic and some hydrophilic. The motivation for this is that any general patterns in the behavior of the ions which may be observed are unlikely to depend on the exact details of the channel architecture and so may reasonably be conjectured to apply to real channels as well. This deduction could not be made from investigations of one channel model alone. Local diffusion coefficients for Na^+ in the same channel models have already been reported elsewhere [28].

That there is likely to be a reduction in the effective mobility of ions in ion channels has been established from various previous MD and experimental studies. In the gramicidin channel it is found experimentally that the mobility of Na^+ is reduced 10–100 times compared to bulk and that of K^+ similarly; the result for Na^+ has been accurately reproduced theoretically [20,23–27, 29,30], though less success has been met with in explaining the behavior of K^+. The reduction in ionic diffusion coefficient D is perhaps not surprising given the strong electrostatic forces that will be felt by the ions. However, reductions in D for ions in uncharged cylindrical hydrophobic channels have also been reported [31] and the mobility of water in channels and channel-like cavities is also found to be reduced [20,32–35], especially as a result of fixed charges in the channel [36,37], even though the water molecule is neutral (though highly polar). The response of water to an external electric field may also be different in a channel compared to the bulk [38].

2. Methods

2.1. Channel models

The channel models were constructed using an *in vacuo* simulated annealing by molecular dynamics (SA/MD) method similar to that described in [39–41]. The model is then solvated, and the ion is introduced by substituting it for a water molecule at the desired initial position. In these models, the lipid bilayer is not included explicitly. The pore region of the channel is fully solvated, and water 'caps' are included at each end of sufficient size to increase the length of the whole simulation system from approximately 30 to approximately 60 Å. All the models were aligned with the pore axis along z, and with the origin approximately at the center of the channel. All the protein chains in every model were patched at the N-terminus by an acetyl group, and (except for alamethicin, which has a C-terminal amino alcohol) at the C-terminus by an NH_2 group.

Diagrams of the channel models, produced using Molscript [42], are shown in Fig. 1, with the protein and water/ion components separated for clarity. The systems studied were:

1. Cubic boxes containing only water and one ion, one of side length 15.6 Å containing 124 TIP3P water molecules and one of side length 31.1 Å containing 999 TIP3P water molecules.
2. An idealized model of a β-barrel, containing Alanine residues only [40] (Fig. 1a). It consists of eight strands (separate, rather than being connected by loops), each 10 residues in length, with a shear number of 8. The barrel has a length of approximately 30 Å, and pore radius of approximately 3.5 Å (all pore radii were calculated using the program HOLE [43]. The system is solvated with 293 TIP3P water molecules in total, approximately 100 (± 5) of them in the pore, and 200 in the caps. This model will be referred to as n8s8.
3. An idealized model of an α-helix bundle, again containing only Alanine residues [39] (Fig. 1b). Each helix is 20 residues in length. The bundle is again approximately 30 Å in length, with a pore radius of approximately 2.0 Å, and when solvated contains 159 TIP3P water molecules, approximately 40 (± 3) of them in the pore. It will be referred to as an5.
4. A model of a real, though artificial, leucine–serine peptide whose channel-forming properties have been the subject of extensive investigation [44–47] (Fig. 1c). The peptide, whose sequence is $(LSSLLSL)_3$, was

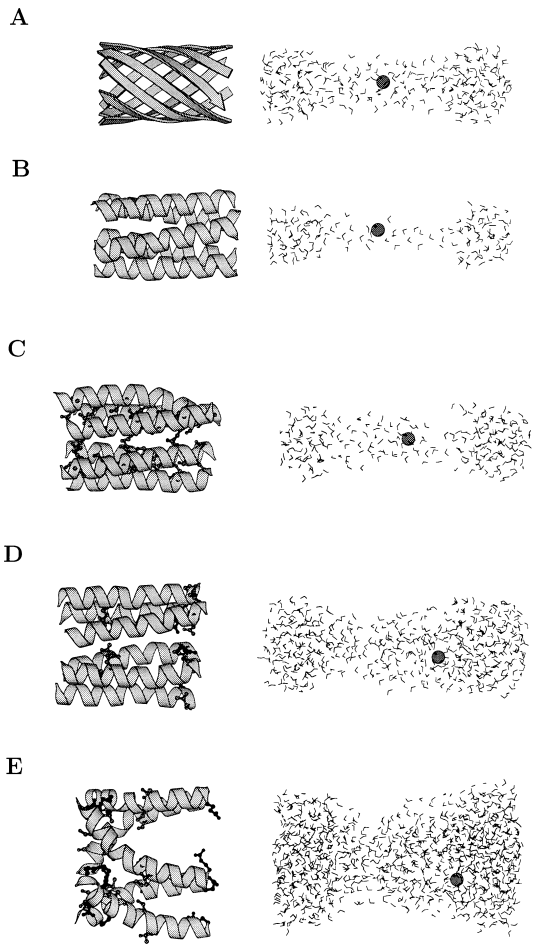

Fig. 1. Diagrams of the various channel models that have been investigated: (a) 8-stranded poly-Ala β-barrel model (n8s8); (b) 5-staved poly-Ala α-helix model (an5); (c) 6-staved Leucine–Serine peptide α-helix model (leu–ser); (d) 6-staved alamethicin α-helix model (alm); (e) $(\alpha 7)_5$ nAChR model. The protein is shown in the left-hand column, with the secondary structural elements in ribbon format, with only polar and ionizable side chains shown explicitly. In the right-hand column the channel and cap water, and the K^+ ion at a typical location, are shown. The water is in bonds-only format and the ion is shown as a van der Waals sphere.

designed to form amphipathic α-helices, and it spontaneously forms inwardly-rectifying channels in lipid bilayers, believed to consist of bundles of α-helices with the serine residues lining an aqueous pore and the leucines directed towards the lipid. Accordingly, the model consists of a helix bundle with the side chains directed as described above. The bundle contains six helices, the number suggested by previous modeling studies [45,48,49] as being the most likely. It has a length of approximately 30 Å, with a pore radius of approximately 3.5 Å in the center of the channel, falling to approximately 2.0 Å near the mouths. It is solvated with 250 water molecules, of which approximately 85 (± 5) lie in the pore. It will be referred to here as leu–ser, though it is also known as LS3 [49].

5. A model of the channel formed by the fungal peptide alamethicin (Fig. 1d), which will be referred to as alm. The sequence of each monomer is UPUAUAQUVUGLUPVUUE-QPhl, where U represents the α-amino isobutyric acid residue [i.e. $-NHC(CH_3)_2CO-$] and Phl represents the phenylalaninol residue [i.e. $-NHCH(C_6H_5)CH_2OH$]. The alamethicin monomer is known to form α-helices [50], and the channels are thought to be helix bundles containing a variable number of monomers, corresponding to the various conductance states of the channels [51–55]. The model studied here is a hexameric bundle, though bundles containing between four and eight monomers have been studied previously [34,56]. The helices have a kink near the central proline, and are aligned such that their hydrophilic faces (defined by Q7) face the pore. The maximum pore radius is approximately 5.2 Å just C-terminal of the center of the channel, falling to approximately 3.0 Å approximately 5 Å in from the channel mouths. It is solvated with 513 water molecules, of which approximately 200 lie in the pore, and it is assumed that all glutamate residues are fully ionized.
6. A model of the pore of the nicotinic acetylcholine receptor (nAChR) (Fig. 1e). The nAChR is the most extensively studied member of the ligand-gated ion channel superfamily [57,58]; it forms pentameric cation-selective channels and is found in the nerve-muscle synapse and in the central nervous system. Of the four transmembrane segments

in each subunit, the M2 segments are believed to form the majority of the lining of the pore [59–63], and structural evidence studies using cryo-EM [12,13] and CD [64,65] suggest, taken together, that the M2 segments are in a centrally-kinked α-helical conformation and form a loose right-handed supercoil with three conserved polar side chains pointing into the pore. The model used here was constructed accordingly. It is a homopentameric helix bundle, with each helix having the sequence EKISLGITVLLSLTVFMLLVAE; this is the sequence of the M2 segment of the neuronal α7 nAChR, which is known experimentally to form homopentameric channels, [66–69]. This model has already been the subject of MD studies [70]. It is approximately 32 Å in length, with a minimum pore radius of ~6 Å, increasing to 18 Å near the helix C-termini. It is solvated with a total of 1026 TIP3P water molecules, of which approximately 430 lie in the pore, and it is assumed that all ionizable residues are in their fully ionized states.

As was mentioned above, the channel models that have been produced were chosen to exhibit a range of secondary structures and types. The an5 and n8s8 models are much simplified relative to real channels, while the alm, leu–ser and nAChR models are built using the sequences of real channels (or, in the case of the nAChR, fragments of real channels).

3. Details of simulations

All simulations were performed using the program CHARMM23 [17] running on Silicon Graphics workstations and servers. The CHARMM PARAM19 parameter set was used, under which aliphatic groups are represented by extended carbon atoms, but polar hydrogen atoms are included explicitly. The water model employed was the CHARMM-modified TIP3P model, which is a three-center non-polarizable model. The Lennard–Jones parameters of the ions were those for the species MK and XCL in the file PARM.PRM of the program QUANTA97 [71]. They are (−0.0100, 2.350) for MK and (−0.2600, 2.060) for XCL, where the first figure is the depth of the minimum in the potential (in kcal mol^{-1}) and the second is the radius where this minimum occurs (in Å).

The ion–water radial distribution functions were calculated and found to be in reasonable agreement with experimental results. The models were minimized for 3000 steps using the adopted-basis Newton–Raphson method, minimizing first the solvent, then the protein under first heavy and then weak constraints. The system was then heated to 300 K over 6 ps using a constant-energy MD scheme with periodic rescaling of molecular velocities, then for the equilibration and production stages of the simulation we switched to using the constant-temperature Nosé–Hoover method [72]. The equilibration stage consisted of two parts, each 8 ps long, and the production stage was 100 ps long. The MD timestep was 1 fs throughout and the lengths of bonds to hydrogen were constrained with the SHAKE algorithm. For each model and each type of ion, this procedure of minimization, heating, equilibration and production was repeated for several (typically nine) initial release positions of the ion in the channel pore and water caps, the ion being initially placed on the channel axis, i.e. at the point (0,0, z_i), for $z_i = \{-20, -15, -10, -5, 0, 5, 10, 15, 20\}$ Å. The total simulation time per model per ionic species was thus 1.1 ns, so the work reported here represents a grand total of 11 ns simulation time. All the production trajectories were sampled every 0.1 ps, so that 1000 coordinate sets for the ion were available for the estimation of D at each point in the channel.

The water in the caps was prevented from escaping by using the MMFP module of CHARMM to put cylindrical or (in the case of the nAChR) hourglass-shaped restraining potentials on it. For consistency with the channel systems, the cubic shape of the water boxes was also maintained with six planar MMFP restraints, rather than by using periodic boundary conditions. The simulations are all thus carried out at constant volume, and though the waters at the surfaces of the caps will have different behavior to bulk water, this is

more likely to affect the behavior of an ion in the caps than in the channel itself for reasons discussed below. Because of the absence of an explicit lipid bilayer (and, in the case of the nAChR model, most of the transmembrane protein), it is also necessary to use restraints to maintain the geometry of the protein: harmonic restraining potentials are placed on the α-carbon atoms (in the case of the nAChR, the Cα atoms near the center of each helix are not restrained). The force constant of the restraining potential was 10 kcal mol^{-1} $Å^{-2}$. Since it was found in the work on gramicidin that the rigidity of the channel can influence the mobility of an ion [29], we have also carried out simulations with weaker harmonic restraining potentials of 0.6 kcal mol^{-1} $Å^{-2}$, which is the force constant that was applied to the methyl spheres that were packed around the gramicidin channel in [27]. The time constant [1/(frequency of harmonic vibration)] of a carbon atom with this restraining potential is 1.5 ps. We also remark that recent simulations of water in alamethicin with an explicit, hydrated lipid bilayer and no structural restraints [73] have found a reduction in the self-diffusion coefficient of *water* which is very similar to what was observed in the present alm model, where lipid was not included [34]. Finally, in the minimization, heating and first equilibration stages of the simulation, a harmonic MMFP restraint was also placed on the *z*-coordinate of the ion, to keep it near its starting position. This restraint was removed for the second equilibration and production stages. Long-range electrostatics were cut off at 13 Å using the force-shift method; given that matter distant from the channel (i.e. lipid and non-pore-lining protein) was omitted, it was considered unnecessary to include long-range electrostatic forces. We believe that the ionic diffusion coefficient and dwell times in the first hydration shell, being the result mainly of local rearrangements in the fluid involving hard-core collisions between the ion and molecules very close to it, are unlikely to be affected much by distant atoms outside the cut-off range (e.g. water in the caps). This would not necessarily be the case with, for example, the energetics of the ion, where long-range electrostatic effects are known to be extremely important.

4. Calculation of effective diffusion coefficient *D*

Our approach to calculating D is based on mean-squared displacement, as was done in [20] for Na^+ in gramicidin, and in [31] for ions in hydrophobic cavities; we use the equation

$$D = \lim_{t\to\infty} \langle (r - \langle r \rangle)^2 \rangle / 2dt \tag{1}$$

where t is the time, $\langle (r - \langle r \rangle)^2 \rangle$ the mean squared displacement from the mean and d the spatial dimension. The $\langle r \rangle$ term corrects for uniform drift in the motion.

It is natural in the case of a homogeneous system to consider the motion in all three spatial dimensions and estimate

$$D \equiv D_r = \lim_{t\to\infty} \langle (r - \langle r \rangle)^2 \rangle / 6t \tag{2}$$

with $r^2 = x^2 + y^2 + z^2$ this equation was used in estimating D in the two water boxes, for example. However, for ions in the channel models we shall consider the motions along and perpendicular to the channel (z-) axis separately, as the character of these motions is different. Therefore, we define

$$D_{\parallel} = \lim_{t\to\infty} \langle (z - \langle z \rangle)^2 \rangle / 2t \tag{3}$$

and

$$D_{\perp} = \lim_{t\to\infty} + \left(\langle (x - \langle x \rangle)^2 \rangle + \langle (y - \langle y \rangle)^2 \rangle \right) / 4t \tag{4}$$

The formal $\lim_{t\to\infty}$ corresponds in practice to fitting the gradient of $\langle (r - \langle r \rangle)^2 \rangle$ vs. t for fairly *short* times (we used the interval 1–6 ps for both, chosen on the basis of inspection of the measured graphs of $\langle (z - \langle z \rangle)^2 \rangle$ vs. t, examples of which are shown below). The expectation value $\langle \cdot \rangle$ is

estimated by averaging over all pairs of ion coordinates in the trajectory that are separated by time interval t. The size of the error bars is estimated by jackknife blocking the trajectory [74]. In most of the trajectories the ion did not move an appreciable fraction of the length of the channel during the production trajectory, so that the D measured can be considered to be a spatially local quantity, $D(z)$ (the z being the average z-coordinate of the ion over the trajectory), in line with the intention of the approach that we are adopting.

It is found even in bulk solution that $\langle r^2 \rangle$ vs. t is not linear but increases rapidly initially, when the ion moves within the shell of its nearest neighbors, and then more slowly at longer times, when motions involving the movement of the ion and solvating waters, coupled with exchange of the waters, become important. These factors depend in a non-trivial way on the size and charge of the ion [75]. The initial gradient of mean squared displacement vs. time (divided by 2, 4 or 6 as appropriate) will be called the local, or cage, or fluid dynamic 'diffusion coefficient' $D_{\parallel}^{(\mathrm{fd})}$ (though the motion is not strictly diffusive on such a short time scale). On this short time scale, one would not expect a large difference between the motion in a channel and in bulk solution, as has been confirmed by the simulations on gramicidin [20].

We have also estimated D in an alternative way, by using the autocorrelation function of the velocity of the ion (Green–Kubo relation)

$$C_v = \langle (v(0) - \langle v \rangle)(v(t) - \langle v \rangle) \rangle$$

$$D = \int_0^\infty C_v \mathrm{d}t \tag{5}$$

as was done in, for example, [20,29] for gramicidin, and in [31]. The decrease in the gradient of mean squared displacement with time corresponds in the case of C_v to a crossing of the time axis followed by a power-law long-time decay which makes accurate numerical evaluation of the integral of C_v difficult [29,76–78]. In our relatively short simulations, random fluctuations quickly come to dominate, and so the upper limit of the integral is cut off in the usual heuristic way, after the second crossing of the time axis (from below), generally at approximately 1 ps.

5. Correlations with water and protein side chains

As was remarked above, the lifetime of water molecules in the first solvation shell of an ion is connected to the ion's diffusive behavior; for example, a longer water lifetime, which increases the effective size of the ion, is thought to be responsible for the low diffusion coefficients of Na^+ and Li^+ compared to K^+, though other effects are also important and a full treatment is quite involved [75]. We have therefore measured this lifetime, where a water is considered to be in the first solvation shell if it is closer to the ion than the first minimum in the ion–water radial distribution function $g_{\mathrm{ion-O}}(r)$ (taken from Koneshan et al. [75]). The lifetime was estimated in a simple way using

$$\tau = \langle n_w \rangle \Delta t / N_{\mathrm{TOT}} \tag{6}$$

where N_{TOT} is the total number of different waters that enter the first solvation shell during the trajectory length Δt and $\langle n_w \rangle$ is the average number in the first solvation shell at any one time. We have not, however, attempted to correlate the exchange of waters from the first solvation shell with the motion of the ion at that instant.

We have also investigated the nature of the interaction between the ion and the channel in the various channel models, by calculating the radial distribution function $g(r)$ between the ion and the protein side chain or backbone atoms. The usual definition (number of atoms in narrow shell at r from ion)/(number of ideal gas atoms of same density in shell at r) causes some problems because the 'density' of the protein is not well defined. Therefore we calculated $N_a =$ (number of protein atoms in narrow shell at r from ion) and $N_b =$ [number of protein atoms in shell at r from ion after ion has undergone a random displacement uniform in $(-5 \ldots +5$ Å)]. Then we used N_a/N_b as an estimate of $g(r)$. The

random displacement decorrelates the ion from the protein, but its size, of the same order as the channel radius, ensures that on average approximately the same number of protein atoms will be found in total.

6. Results

6.1. Local mobility in channels

We first analyze the motion of the K^+ and Cl^- ions in the channel models. In Fig. 2 the z-components of the ion trajectories for the K^+ ions in each channel are shown as a function of time. Generally the motion seems to be diffusive or drift-plus-diffusive, but there are some exceptions; for example, the ions that start near the ends of the narrower an5 and leu–ser channels seem to be 'squeezed out', tending to move out rapidly during the equilibration stage of the simulation. More detailed investigation of this will require free energy calculations, but it is presumably related to the narrowness of the channels at the ends, and the proximity and exposure of the helix backbone dipoles in these regions. There is a clear 'drift' of the ions in the channel only in the case of alamethicin, where the ions move towards the C-terminus, (positive z), as might be expected due to both the direction of the α-helix dipoles and the presence of a ring of negative charge produced by glutamate residues at approximately $z = 10$ Å. The trajectories of Cl^- ions (data not shown) display several of the same qualitative features; again, the ions are not stable near the ends of the leu–ser model, and drift is observed in the alm model, this time from positive to negative z (towards the N-termini), in line with the charge reversal.

Some representative graphs of the resulting mean squared displacements in the z-direction are shown in Fig. 3. We show results for the potassium ion released at $z = \{-20, -10, 0, 5, 20\}$ Å for leu–ser. It is apparent that the mean squared displacement is sometimes convincingly linear, but at other times not. This is probably a consequence both of real deviations in z^2 vs. t at longer times due to the effect of the channel

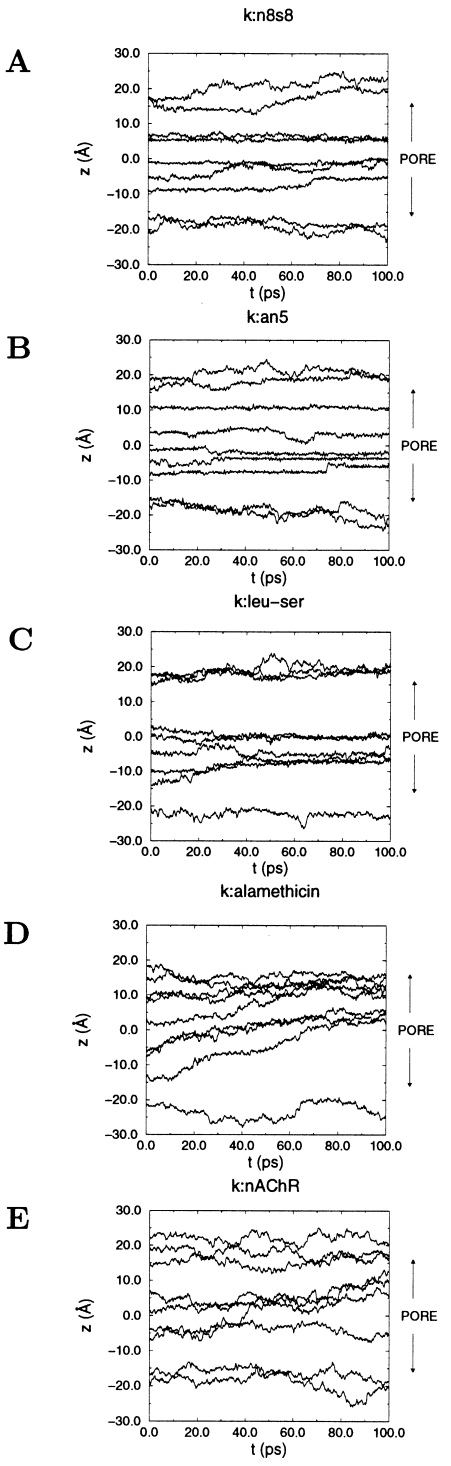

Fig. 2. z-Component of K^+ ion trajectories for: (a) n8s8; (b) an5; (c) leu–ser; (d) alm; and (e) nAChR.

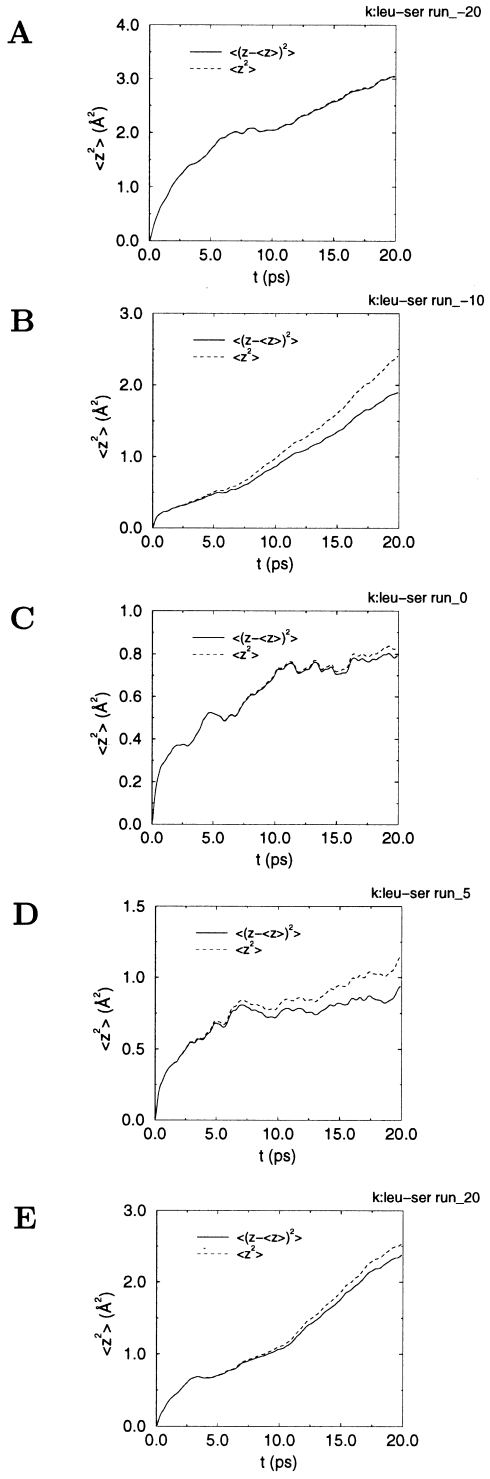

protein and also of inadequate sampling; the entire trajectory of an ion is only five times longer than the maximum interval shown here, 20 ps. We emphasize that the process of fitting over 1–6 ps produces only a local mobility; it does not necessarily give an indication that this effective mobility can be used alone to describe the behavior over longer time intervals.

The corresponding trajectories in the x,y plane are shown in Fig. 4. The restraining of the ion by the walls of the channel is clearly apparent, as is the fact that the ion generally remains near to the channel axis (which is at the origin). These trajectories are qualitatively similar in the other narrow channels (an5 and n8s8). In these channels, the greater mobility in the caps compared to the pore is apparent from the ion trajectories, Figs. 2 and 4, alone; for the wider alm and (especially) nAChR models, the trajectories in the channel resemble those in the caps more closely, being indistinguishable in the case of the nAChR. There is little difference between potassium and chloride, except that the chloride seems to prefer an off-axis location in the narrow channels.

The local diffusion coefficients have been calculated for both ionic species in all the channels. The results are shown in Figs. 5 and 6 for K^+ and Fig. 6 for Cl^-. The graphs also show the effective radius of the channel as a function of axial position, as estimated by the program HOLE [43]. For comparison, in the simulations on the ions in the two water boxes of different sizes, it was found that $D_r(K^+,\ L = 15.5\ \text{Å}) = 0.16(3)\ \text{Å}^2\ \text{ps}^{-1}$ and $D_r(K^+, L = 31\ \text{Å}) = 0.21(4)\ \text{Å}^2\ \text{ps}^{-1}$ while $D_r(Cl^-, L = 15.5\ \text{Å}) = 0.18(5)\ \text{Å}^2\ \text{ps}^{-1}$ and $D_r(Cl^-, L = 31\ \text{Å}) = 0.21(2)\ \text{Å}^2\ \text{ps}^{-1}$.

The error bars on the diffusion coefficients from channel simulations (shown at 1 S.D.) are quite large, but there is generally a very clear

Fig. 3. Graphs of $\langle (z - \langle z \rangle)^2 \rangle$ vs. t for K^+ ion in the leu–ser model at: (a) $z = -20$; (b) $z = -10$; (c) $z = 0$; (d) $z = 5$; and (e) $z = 20$. Note that the labels (run 10, etc.) refer to the z-coordinate of the ion at its release, not to the point to which it moved, and that the vertical scale is different on the different graphs.

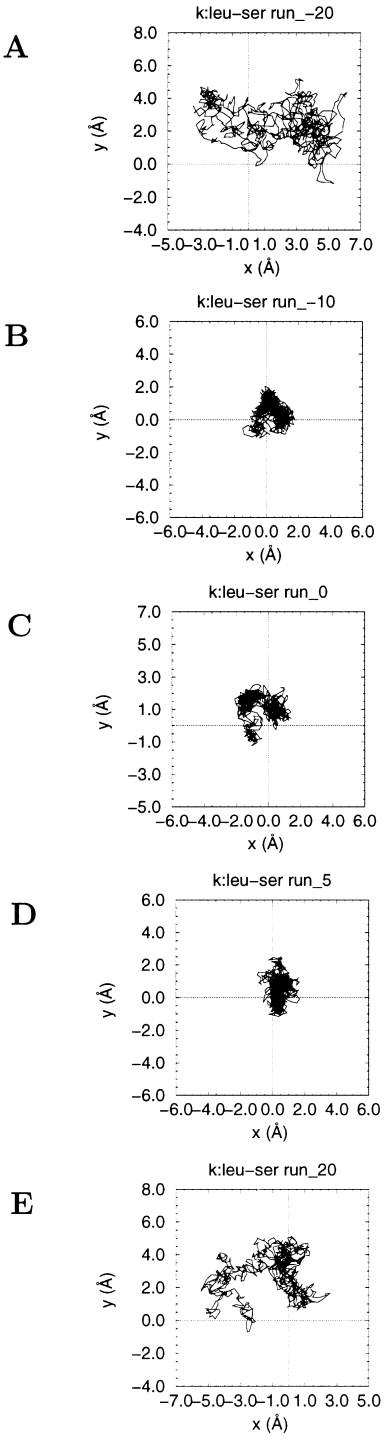

reduction in local mobility in the pore regions of the an5, n8s8 leu–ser and (to a lesser extent) alm models. This is more consistent and pronounced for $D_{\perp}$ than $D_{\parallel}$, but is apparent for both. The largest reductions in $D_{\parallel}$ are observed in the narrowest channel, an5, with the more hydrophilic leu–ser channel showing smaller reductions and the alamethicin channel, which is both more hydrophilic and wider, smaller reductions still. Within the error bars, the mobility of K^+ and Cl^- seem to be reduced by similar amounts. In the case of the nAChR, however, there is no evidence of reduced local mobility of either ionic species in the channel, in contrast to Na^+, for which a small reduction did appear to occur [28]. Within a particular channel, the effective diffusion coefficient tends to follow the pore radius profile, e.g. the local maximum of mobility of both ions in the leu–ser channel at $z \approx -2$, but this is quite dependent on the nature of the pore lining; e.g. $D_{\parallel}$ has a maximum in a narrow part of the alm channel at $z \approx 8$.

It is notable for both ionic species that the mobility is generally less in the caps of the an5, n8s8 and leu–ser models than it is in the caps of the alm model or the nAChR. This is probably due to the larger size of the caps in the latter models; they have a radius of approximately 18 Å compared to approximately 12 Å or less than 10 Å (n8s8, an5). D was also found to be correspondingly smaller in the $L = 15$ Å water boxes.

6.2. Confirmatory tests

We now present some confirmatory and subsidiary results for the dynamic behavior in the channel. First we show the behavior of the short-time local fluid dynamic 'diffusion coefficient' $D_{\parallel}^{(fd)}$ for K^+ in leu–ser (with 10.0 kcal mol^{-1} $Å^{-2}$ restraints), calculated from z-displacement

Fig. 4. The trajectory of K^+ ion in the (x,y)-plane in the leu–ser model at: (a) $z = -20$; (b) $z = -10$; (c) $z = 0$; (d) $z = 5$; and (e) $z = 20$.

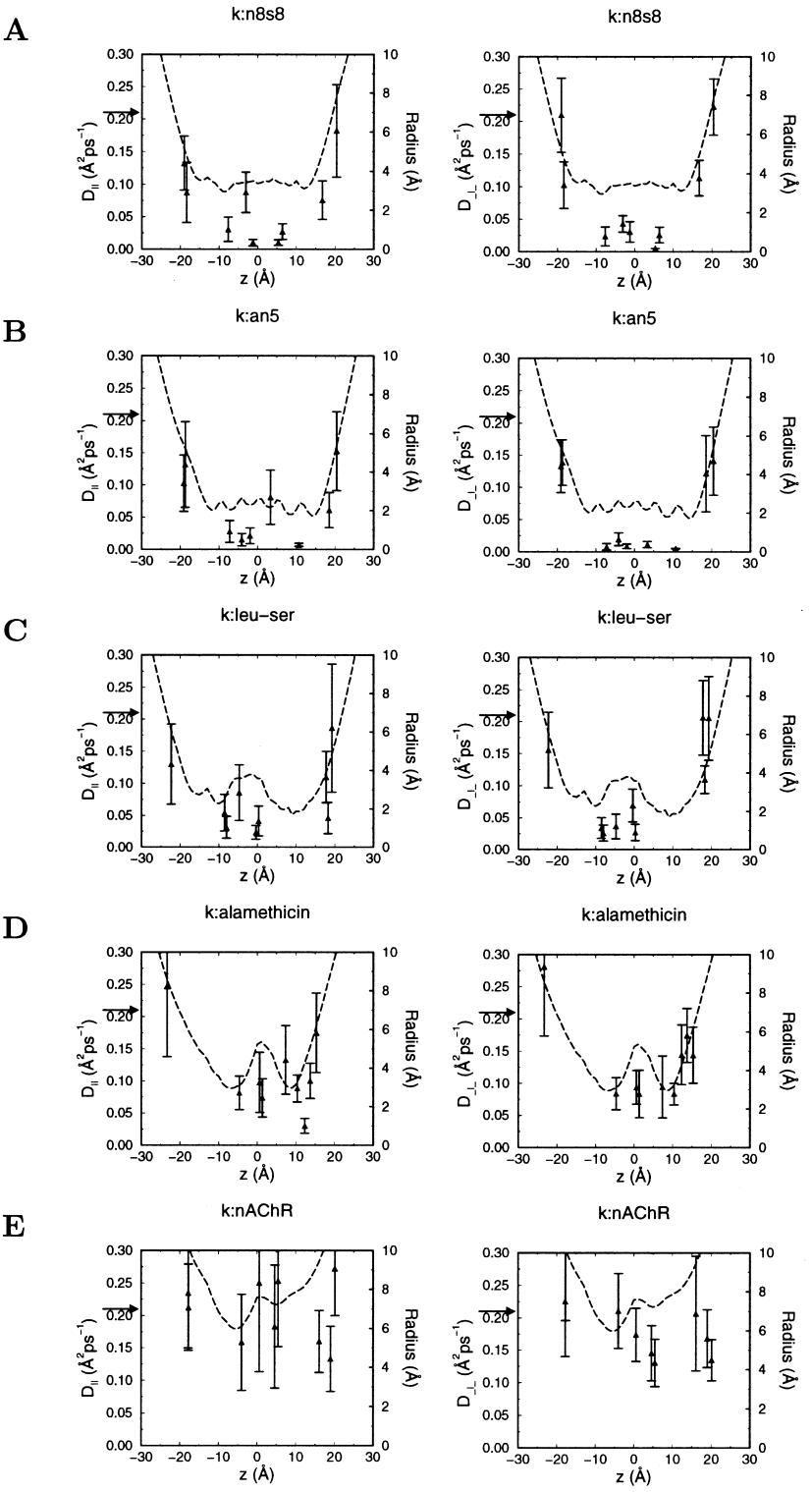

Fig. 5 legend overleaf

between 0 and 0.5 ps (Fig. 7a). As described in the section on the calculation of effective diffusion coefficient above, this comes from the initial gradient of $\langle (z - \langle z \rangle)^2 \rangle$ vs. t (Fig. 3), describing motion of the ion on very short time scales, while within the 'cage' of its nearest neighbor water molecules. This initial gradient is much larger than its subsequent values, and much less dependent on position in the channel, and accordingly $D_{\|}^{(fd)} \sim 0.40$ Å ps^{-1}, much larger than $D_{\|}$.

The effects of varying the strength of the restraining potentials on the helix backbone atoms will now be described. This test was done by running simulations for K^+ and Cl^- in leu–ser with α-carbon restraining forces of 0.6 kcal mol^{-1} Å^{-2} instead of 10.0 kcal mol^{-1} Å^{-2}. In Fig. 7b we show the z-displacement of the potassium ions (cf. Fig. 2c) and in Fig. 7c,d, the effective diffusion coefficients of K^+ and Cl^-, respectively, from fitting $\langle (z - \langle z \rangle)^2 \rangle$ vs. t between 1 and 6 ps. These should be compared with Fig. 5c and Fig. 6c, which are the corresponding results with stronger restraining potentials. The ions are a little more stable near the mouths of the channels but the qualitative features of $D_{\|}$ remain the same, and sometimes even quantitative features are similar, e.g. the peak in $D_{\|}(K^+)$ at $z \approx -5$ Å. The largest differences (though still within the error bars) actually seem to be observed for the ions in the *caps*, where it is very unlikely that they are the result of the restraining potentials on the helices. We remarked in the previous section that the diffusion coefficient in the caps of the leu–ser model tends not to attain its bulk solution value, because the caps themselves are still quite small. For the simulations with the weaker restraints, we have also calculated the effective diffusion coefficients from the velocity autocorrelation function (VACF) of the same ionic trajectories, using Eq. (5). Error bars were calculated by blocking. The results, shown in Fig. 7e,f, are similar to those calculated from mean square displacement (c,d) within the error bars, and thus provide support for the use of the mean square displacement method in the rest of the simulations. In fact, it appears from the Cl^- trajectory that there is some evidence that use of the VACF discriminates the pore from the cap rather better than the mean squared displacement does.

6.3. Interaction with the channel surface

The radial distribution functions $g(r)$ between ion and protein are shown in Fig. 8 (results for K^+ on the left and Cl^- on the right). $g(r)$ was calculated for the protein side chain and backbone atoms separately, giving $g_{ion-sch}(r)$ and $g_{ion-bb}(r)$, respectively. The results are averages for all ion trajectories that lay completely within the channel pore, which we took to be those for which -10 Å $< \langle z \rangle < 10$ Å.

Considering $g_{ion-sch}(r)$ first, it seems clear that both types of ion can approach the side chains in leu–ser (Fig. 8c) and alm (Fig. 8d) to approximately 2–2.5 Å, corresponding to direct contact between ion and atoms in the side chains (it is approximately 1 Å less than the sum of the van der Waals radii), whereas in the hydrophobic channels an5 and n8s8, the ions remain slightly further from the side chains, notwithstanding the fact that these channels (particularly an5) are narrower. This suggests that polar atoms in the side chains can momentarily replace water in the first solvation shell of the ion, but hydrophobic atoms do not do this to such a great extent. This is confirmed by inspection of 'snapshots' from the trajectories, and is in broad agreement with the results of [31]. In the polar channels, $g_{ion-sch}(r)$ for K^+ lacks the small peak around $r = 2$ that is observable for Cl^-; this is a result of the coordination of Cl^- by polar H atoms, which of course does not occur for K^+. In general, the ability of

Fig. 5. Diffusion coefficients of K^+, as a function of average z-position of the ion for: (a) n8s8; (b) an5; (c) leu–ser; (d) alm; and (e) nAChR, estimated by fitting the gradient of mean squared displacement between 1 and 6 ps for ions placed initially on the channel axis, at various points along it. In the left-hand column is $D_{\|}$ from fitting $\langle (z - \langle z \rangle)^2 \rangle$ vs. t, in the right-hand column $D_{\|}$ from fitting $\langle (x - \langle x \rangle)^2 \rangle + \langle (y - \langle y \rangle)^2 \rangle$ vs. t. As well as the diffusion coefficients (solid triangles with error bars), the figures also show the effective radius of the channel as a function of axial position (broken line), as estimated by the program HOLE. The values of $D_r(K^+)$ from the $L = 31$ Å boxes (≈'bulk solution') are indicated with arrows (→) on the left vertical axis.

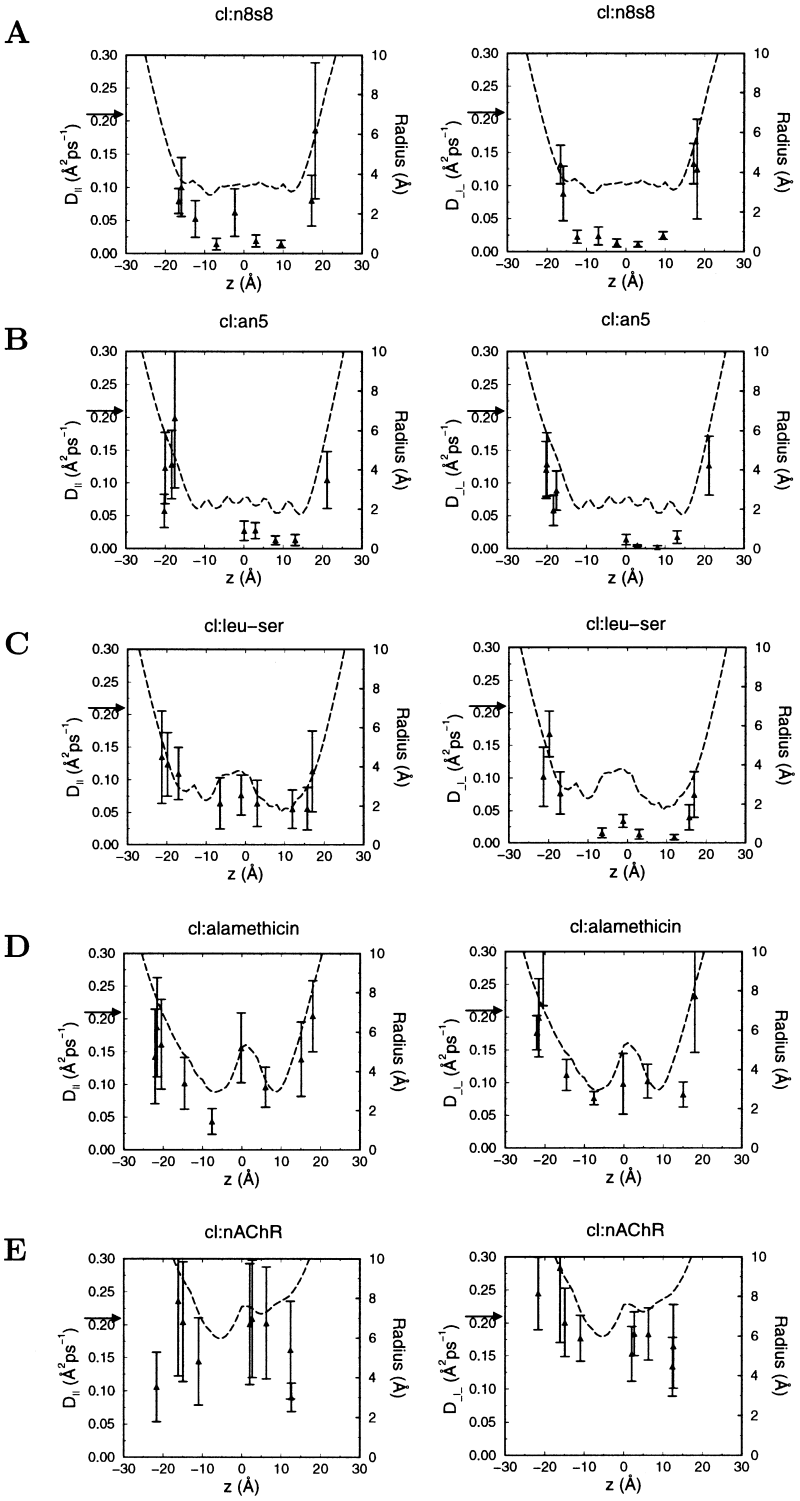

Fig. 6. Diffusion coefficients of Cl^-. Other details as for Fig. 5.

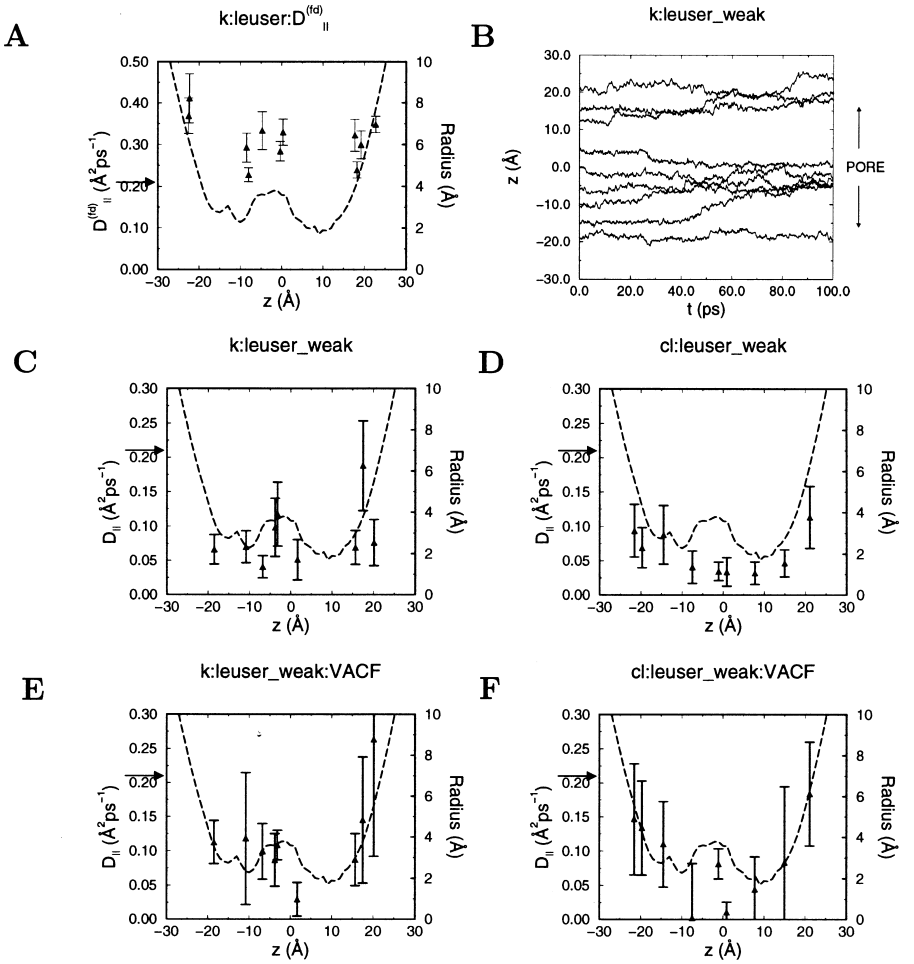

Fig. 7. Results of confirmatory tests: (a) is for the leu–ser model with 10 kcal $mol^{-1}Å^{-2}$ C_α restraints, while (b–f) are for the leu–ser model with 0.6 kcal $mol^{-1}Å^{-2}$ C_α restraints. (a) Short-time local or fluid dynamic 'diffusion coefficient' $D_\parallel^{(fd)}$ from motion in the z-direction as a function of average z-position of the ion for K^+ in leu–ser, estimated by fitting the *initial gradient* of $\langle (z - \langle z \rangle)^2 \rangle$ vs. t between 0.1 and 0.5 ps. (b) z-Component of K^+ ion trajectories. (c) Diffusion coefficient $D_\parallel$ of K^+ and (d) $D_\parallel$ of Cl^- for ions in leu–ser with weak (0.6 kcal $mol^{-1}Å^{-2}$) C_α restraints. (e,f) $D_\parallel$ calculated from velocity autocorrelation function C_v for K^+ and Cl^- in the same weakly restrained leu–ser model. In (a,c–f) the diffusion coefficients are solid triangles with error bars, the broken line is the effective radius of the channel as a function of axial position as estimated by the program HOLE, and the values of $D_r(K^+)$ from the $L = 31$ Å boxes ($\approx$'bulk solution') are indicated with arrows ($\rightarrow$) on the left vertical axis.

ions to make direct contacts with polar side chains is consistent with the role that they are believed to play in ionic selectivity. $g_{ion-sch}(r)$ for K^+ in the nAChR (Fig. 8e) also shows a tendency to decrease to zero at an appreciable distance from the channel wall, but this is probably a consequence of the release point on the axis in this channel, which has much the largest diameter. It is not very similar to the hydrophobic channels, for which $g_{ion-sch}(r)$ increase from zero more rapidly and then decrease again at larger r. The chloride ion, however, does approach polar side chains in the nAChR closely, as for the other polar channels; and in [70], the same behavior was observed for a Na^+ ion that was released in an off-axis position.

The behavior of $g_{ion-sch}(r)$ at larger r is also interesting. It has some structure in all the chan-

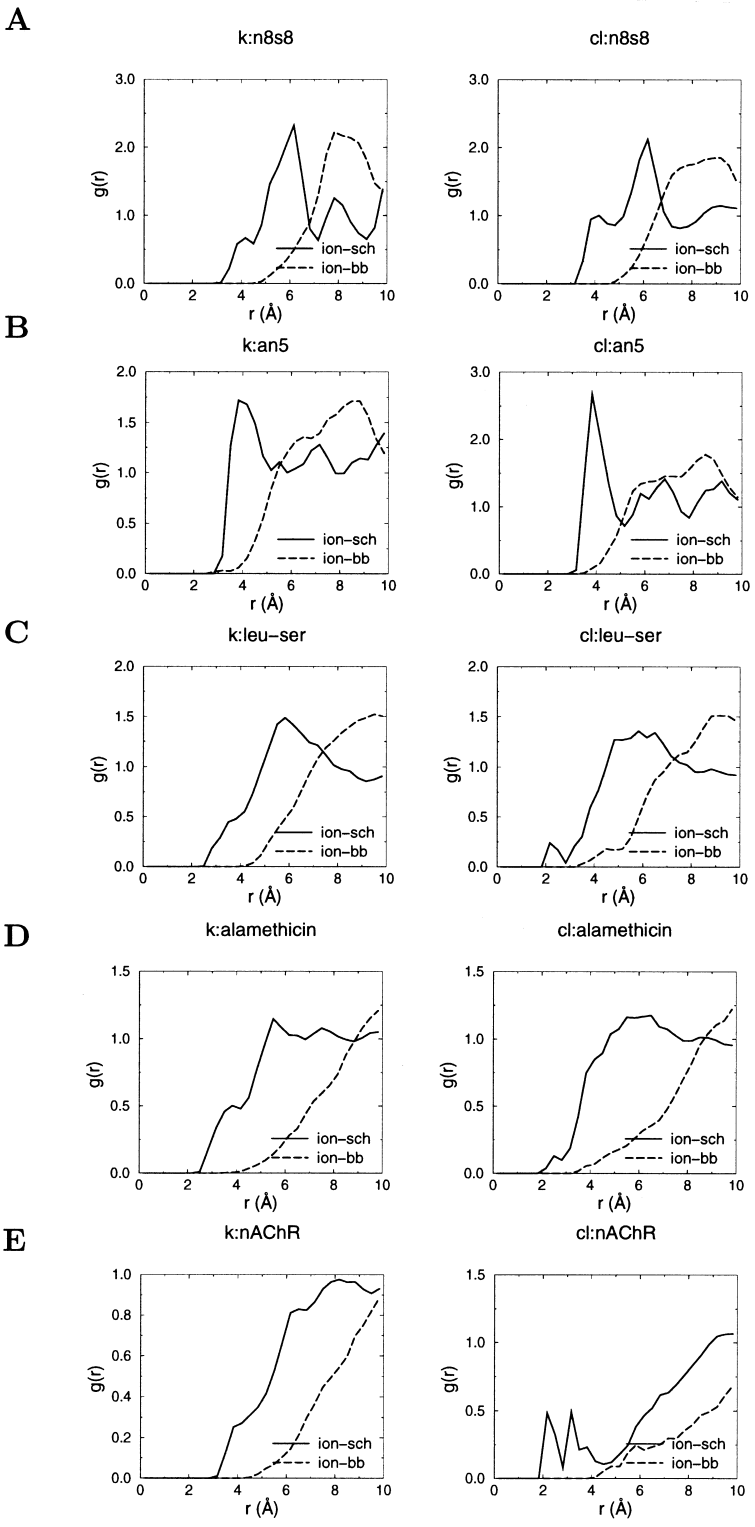

Fig. 8 legend overleaf

nels, particularly the an5 and n8s8 channels, where it has well-defined secondary minima and maxima, though these are less pronounced than was previously found for Na^+. These would not be observed if the ion was diffusing freely in z; their presence is evidence of local free energy minima due to the protein.

There is rather less variation in $g_{ion-bb}(r)$ between the different models than in the shape of $g_{ion-sch}(r)$. The most important feature of $g_{ion-bb}(r)$ is that, within the channel proper, it generally goes to zero at approximately 5 Å for the n8s8 (beta-barrel) model, and at approximately 4 Å for the other helix-bundle models. Thus it does not appear that there is direct interaction between the ion and the backbone in any channel, in contrast to the case of gramicidin, where coordination of the ion by backbone carbonyl groups is of overriding importance in permeation [16,25,79]. Here, it is the side chains that form the lining of the channels. The an5 model is an exception to this, having some very small density between ion and backbone at $r \leq 4$ Å for both ions within the channel. while the leu–ser and alm models have some density at $r \leq 4$ Å for chloride only. Ions can, however, approach backbone atoms more closely at the ends of the helices, emphasizing the exposure of the backbone in these regions; for example, the K^+ released in an5 at $z = 10$ Å spends moves quite rapidly to $z \approx 17$ Å, where it remains close to an accessible backbone C=O, producing a large peak of $g_{ion-bb}(r)$ at $r \approx 3$ Å. This has already been commented on above, in the discussion of Fig. 2.

6.4. Lifetimes of water in the first solvation shell

In Fig. 9 we show both the average number $\langle n_w \rangle$ and the lifetime τ of water molecules in the first solvation shell [calculated from Eq. (6)], as a function of $\langle z \rangle$ for the ion. In the wider nAChR and alm models there is little variation with z, with $\langle n_w \rangle \approx 8$ for K^+ and ≈ 9 for Cl^-, and $\tau \approx 10$ ps for both. This latter value is in reasonable agreement with values in [75] of $\tau = 14.3$ ps for K^+ and $\tau = 16.7$ ps for Cl^- estimated for bulk solvent, especially since the estimate from Eq. (6) will tend to underestimate the lifetime in comparison with an analysis based on the decay of correlation functions. However, it is in any case the variation in τ between models and as a function of z that is of greater significance here.

Similar values of τ and $\langle n_w \rangle$ to those in alm and the nAChR are found in the caps of the other models, but in the channel regions some differences are observed. In n8s8 and leu–ser, $\langle n_w \rangle$ is not reduced except at the narrow C-terminus of leu–ser for Cl^-, but τ is increased to approximately 30 ps in the channels for both species. In the very narrow, and hydrophobic, an5 channel, τ increases to 60–70 ps in the center of the channel, (this is likely to be strongly underestimated as it is close to the total length of the trajectories), while the coordination number $\langle n_w \rangle$ is reduced to approximately 6.

7. Discussion

7.1. Models and simulation techniques

Of the models used here, leu–ser, alm and nAChR represent 'real' channels and so some discussion of their likely accuracy is called for. For none of these channels is there a high-resolution structure of the intact pore. For alamethicin, there is an X-ray structure of a single helix [50], which guided our modeling, and it seems likely that the hexameric structure used here exists, given the experimentally-observed conductance states found in channels formed of alamethicin monomers and covalently-linked dimers [54]. Furthermore, unrestrained MD simulations in a fully hydrated bilayer have revealed that the hexameric alamethicin helix bundle is stable on at least an

Fig. 8. Radial distribution functions $g_{ion-sch}(r)$ and $g_{ion-bb}(r)$ between the ion and protein side chain (solid lines) and backbone (dotted lines) atoms for (a) n8s8; (b) an5; (c) leu–ser; (d) alm; and (e) nAChR. The results for K^+ are on the left, and for the Cl^- on the right, and are averages for all ionic trajectories with $-10 < \langle z \rangle < 10$.

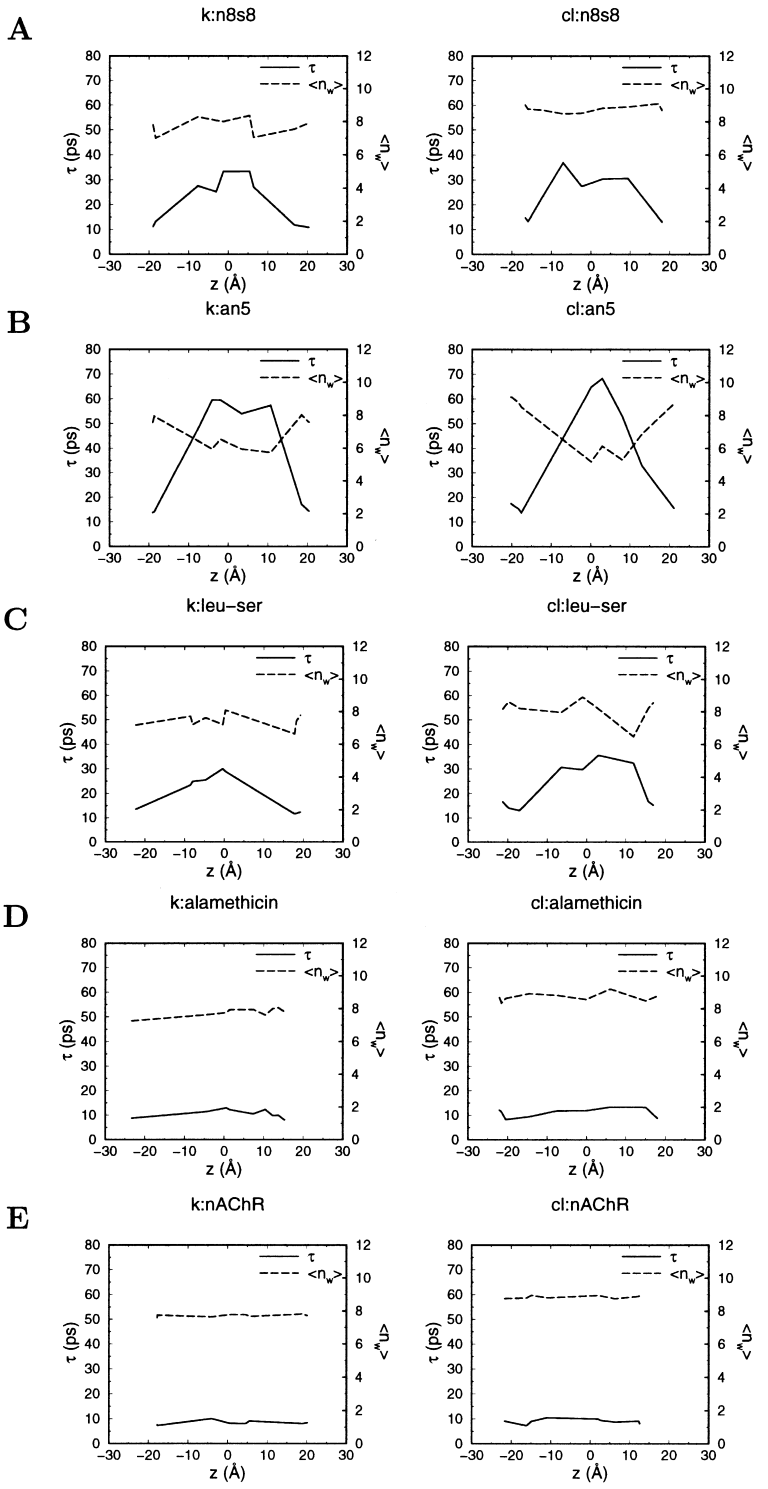

Fig. 9 legend overleaf

approx. 15-ns timescale (Sansom and Tieleman, unpublished observation).

The leu–ser model is plausible given that this peptide was *designed* to form amphipathic helices, which would then associate to form channels with a hydrophilic lining and hydrophobic exterior, though details such as the precise nature of the helix packing might not be correct. The nAChR model presents the opposite problem to alm; the degree of oligomerization is known, but not the structure of each element. However, our model is in reasonable agreement with most point mutagenesis and cryo-EM [12,13] data, and also with other putative structures that have recently been proposed for the M2 helix bundle [80,81]. As for alm, the nAChR model does not take into account pK_A shifts of ionizable residues that may occur [82]. Neither does it include the other transmembrane protein segments M1 (some of which is thought to contribute to the lining of the pore [62,63]), M3 and M4. We believe that the present model represents almost all of the receptor that can be modeled with confidence at the present stage of knowledge; it will be improved as higher-resolution structural data becomes available.

The omission of M1, M3 and M4 in the nAChR can usefully be discussed together with the omission of explicit lipid and other ions in all five channel models. Without the lipid and other protein elements, the protein that is included in our models would be unstable, were it not for the use of the restraining potentials. However, the omission of these elements is, we believe, likely to have a much smaller effect on mobility than it would on, for example, the ion's average energy or free energy in the channel. The rigidity of the channel was found to be important in gramicidin in [29], but the simulations carried out here with weaker positional restraints on the backbone showed that that factor was less important for these channel models. Such restraints would be expected to be more influential in the case of gramicidin, where the ion is coordinated by backbone C=O groups, than in the channels studied here, where it interacts instead with the (unrestrained) side chains and not directly with the backbone. The calculations of $g_{\mathrm{ion-sch}}(r)$ and $g_{\mathrm{ion-bb}}(r)$ corroborate this. We remark that the extensive desolvation in the gramicidin channel seems to be quite unusual, though it may occur in short segments of other channels (for example the putative selectivity filter of the KcsA potassium channel [3]).

The omission of other ions will have several effects. Firstly, these simulations have been carried out at 'infinite dilution', i.e. with only one ion in the pore at a time. From electrophysiological evidence, many ion channels (such as Ca channels and K_{ir} channels), are thought to be multi-ion pores [2]; their behavior is understood in terms of barrier-hopping rate theory models where an incoming ion is necessary to displace another from a 'binding site' in the channel, a process that, repeated, leads to permeation. The same effect is described in a different way by including the time-averaged density of permeant ions in Poisson–Nernst–Planck calculations (where it affects all channels, even those described as 'single-ion pores' in the barrier-hopping picture). At the moment, it is envisaged that these effects will be added in a perturbative fashion in the 'reduced model' stage; but simulations in full-atomistic detail containing more than one ion may be necessary. Secondly, it is of course the presence of other ions that produces the membrane potential that drives perturbation; this, however, may certainly be considered a 'small perturbation' and added in later. Thirdly, recent work [83] has demonstrated that explicit counterions are necessary for the stability of certain proteins in unrestrained simulations. Here, however, the secondary structure will be maintained by the structural restraints used. The simulation protocol

Fig. 9. Lifetime of waters (τ) and number of water oxygens (N_w) in the first solvation shell of the ion (defined by the position of the first minimum in $g_{\mathrm{ion-O}}$) for (a) n8s8; (b) an5; (c) leu–ser; (d) alm; and (e) nAChR. The results for K^+ are on the left, and for the Cl^- on the right.

adopted, and the likely effect of elements of the channel that are omitted, are discussed in more detail in [28].

We now turn from a consideration of the channel models to comment briefly on the mean-squared displacement method used to estimate D. In other work the use of the velocity autocorrelation function has been preferred, but our tests suggest that, at least on the short timescales investigated here, the two give equivalent results.

Finally we comment on the approach of tackling the problem by attempting a separation into a 'diffusion coefficient' and a 'position dependent free energy', i.e. to regard the ion permeation problem as a walk over a free energy surface, where the 'step size' of the walk is described by the local mobilities/diffusion coefficients that are the subject of this paper, and the motion of the ions is directed by the gradient of the local free energy surface. Thus, the effective local mobility would describe the driving forces on the ions from the water; this mobility could then be used in a simplified model which no longer included water explicitly (its average effect, and that of the protein, would be handled by a potential of mean force). This approach is very similar to that adopted in the derivation of the Langevin equation. Any difference between D in the bulk and in the channel would then come from the confinement (and, perhaps, orientation) of water in the channel; the water produces a local potential well at the ion's present position which must relax before the ion can move any appreciable distance. The extent of the water's confinement will influence this relaxation and thus the ion's ability to move. In this study the ion did, of course, feel the effect of the channel protein and this will have had some biasing effect on the measured local mobilities (tending to reduce them). It is difficult to disentangle the effects of the (as yet uncharacterized) free energy surface from those of confinement; on sufficiently long length (or time) scales the potential due to the channel, which we shall call Φ_{ch}, will dominate, which is one reason for our concentration on small time scales. As a consistency check, we comment that on the 6-ps timescale, with $D = 0.1$ Å^2 ps^{-1} the r.m.s. z-displacement of the ion is just over 1 Å whereas the pitch of α-helix, which gives the typical length scale for variation of the local potential Φ_{ch}, is approximately 5.4 Å. For the mean squared displacement to be an accurate measure of mobility, the departures from linearity of Φ_{ch} should be small (i.e. at most $\sim$ RT) over the length scales studied. While the r.m.s. displacement is smaller than the period of an α-helix, it is not very much so, and there will probably be components to Φ_{ch} which have a still more rapid spatial variation, particularly near charged side-chains. It is apparent, then, that the ion's motion is unlikely to be truly unaffected by Φ_{ch}, even on the 6-ps timescale, so our results represent an upper limit on the effective diffusion coefficient on this timescale and may need to be reinterpreted when the free energy surface has been characterized.

However this may be, we emphasize that, because we are regarding the free energy as a quantity to be measured separately, the quantities that we define as D, coming from fitting over 1–6 ps, are not the same as the 'effective diffusion coefficient' that applies in, for example, the equation

$$P = D'_{\text{eff}} A/L$$

where P is the channel permeability, L its length and A its cross-sectional area. The effect of the potential due to the channel protein Φ_{ch} is here entirely subsumed into D'_{eff} The same is true of D''_{eff} in the equation

$$D''_{\text{eff}} \approx k \Delta L^2$$

where k is the barrier crossing rate over one of the fundamental barriers which make up the gramicidin channel, and was measured directly by a MD technique designed to sample barrier crossing configurations [26].

7.2. Comments on results

Before beginning a detailed discussion, we remark that the results presented here should be interpreted in terms of the difference between channel and bulk environments, rather than as

absolute values, although we found that in the larger water boxes $D_r = 0.21(4)$ Å^2 ps^{-1} for K^+ and $D_r = 0.21(2)$ Å^2 ps^{-1} for Cl^-, which are in fact in close agreement with the experimental values of 0.196 Å^2 ps^{-1} and 0.203 Å^2 ps^{-1}, respectively. They are also close to the values of 0.20 Å^2 ps^{-1} for both species in bulk SPC/E water, from [31].

Apart from the gramicidin simulations, the only other measurements of D for K^+ and Cl^- in an ion channel by simulation, as far as we are aware, are those of [31] for a cylindrical hydrophobic cavity of 3 Å radius; this thus bears some resemblance to the leu–ser, an5 and n8s8 models, though quantitative agreement cannot be expected. It was found that $D_{\|}(K^+)$ was reduced to 0.04(1) Å^2 ps^{-1} and $D_{\|}(Cl^-)$ to 0.07(1) Å^2 ps^{-1}. These reductions are comparable with, though slightly smaller than, those found here (e.g. for K^+, 0.002(2)–0.09(5) Å^2 ps^{-1} in an5, typically 0.02(2) Å^2 ps^{-1}, 0.02(1)–0.08(5) Å^2 ps^{-1} in leu–ser; for Cl^-, 0.005(3)–0.10(6) Å^2 ps^{-1} in n8s8, 0.02(1)–0.11(8) Å^2 ps^{-1} in leu–ser). In particular, we generally observe similar behavior for the two species within the error bars. The reduction in mobility is accompanied in the narrower channels by a slowing of the exchange of water molecules from the first solvation shell, shown by an increase in the dwell time τ; however, there also seems to be a reduction of $D_{\|}$ to approximately 0.10 Å^2 ps^{-1} in the alm model, where no clear increase in τ is observed.

In comparison with the behavior of Na^+ in the same models [28], the mobilities of potassium and chloride are reduced to a similar or greater extent in the narrow channels, but while there was evidence for a small reduction in $D(Na^+)$ even in the nAChR model, there is no suggestion of such behavior for potassium and chloride. The fractional reduction in mobility of the ions is however rather smaller than that of *water* in channels [20,32–35,70].

In the large literature on simulations of gramicidin, less attention has been paid to potassium ions than sodium, and still less to chloride (to which, of course, gramicidin is not permeable). There has been some work on large cations [84]. The results of simulations on potassium ions have also been rather less successful than for sodium, predicting a relatively small reduction in mobility in the channel, which would imply a much larger potassium permeability than is observed experimentally. In [26] an effective diffusion coefficient of 0.097 Å^2 ps^{-1} is estimated from the response to an external field, while measurements of the autocorrelation function of the force on a tethered ion give 0.057 Å^2 ps^{-1}. In [85] D for K^+ in gramicidin is estimated to be 0.09 Å^2 ps^{-1}, estimated from the response to an external field, i.e. from a measurement of the mobility.

Aside from the studies on gramicidin and the work of Lynden–Bell and Rasaiah, other estimates of effective diffusion coefficient of ions in channels have tended to come from two sources. One is fitting to experimental permeabilities, the results of which are not directly comparable with ours because they fold the effects of potential barrier crossings and access resistance into the mobility; the value of D estimated this way is 1.8×10^{-3} Å^2 ps^{-1}. The other is the fitting of parameters to experimental I–V curves. For example, in [15], ionic diffusion coefficients (and other parameters) are fitted using the Poisson–Nernst–Planck equation to a large amount of current–voltage data for the leu–ser peptide. There, it is estimated that D for K^+ is reduced 10-fold and for Cl^- 100-fold, whereas we see a reduction of approximately 2–10-fold for both species depending on position in the channel. This indicates that the reason for the experimental selectivity of the leu–ser peptide channels for potassium over chloride must reside elsewhere, probably in the different free energies of the ions in the channel.

With regard to the calculations of $g_{\mathrm{ion-sch}}(r)$ and $g_{\mathrm{ion-bb}}(r)$ and the solvent coordination number in the channel, we remark that the observed direct interaction between ions and side chains in channels with a polar lining, is what might be expected to be necessary if polar side chains play an important part in ion selectivity, as has been suggested for leu–ser and the nAChR [60,67,68]. However, while the present results are consistent with that idea, quantitative investigation will require free energy calculations. Moreover, these interactions do not produce a clear change in

coordination number of the ion, (which occurs only in the very narrow an5 channel), so they must be viewed as occurring only occasionally [consistent with the small magnitude of $g_{\mathrm{ion-sch}}(r)$].

8. Conclusion

It is found that the short-time effective diffusion coefficients of potassium and chloride ions in various ion channel models is reduced relative to bulk solution. The largest reduction is observed in the narrowest channels, so that in the an5 model (a pentameric bundle of poly-alanine α-helices) for example they are reduced at least tenfold, while a reduction of approximately 50% is observed in wider pores, like that of a model of the fungal peptide alamethicin. We see no reduction, however, in the largest pore studied, that of a model of the M2 helix bundle of the nicotinic acetylcholine receptor. The observed reductions in D are associated with a slowing down of the exchange of water from the ion's first solvation shell and, in the narrowest channels, with a reduction in the extent of hydration. These results are broadly consistent with previous studies of sodium ions in these models [28] (except that here a small reduction occurred in the nAChR as well), and with a study of ions of various kinds in cylindrical hydrophobic cavities [31].

The decrease in effective diffusion coefficient seems to occur regardless of the secondary structure of the channel, as the channel models include examples of what are thought to be the two most common secondary structure motifs, β-barrel and helix-bundle channels, and a large reduction in mobility is observed in both. However, the strong dipole field in the helix-bundle channels, especially when augmented by charged ionizable groups as in the case of alamethicin, produced a directional drift of the ions which was not observed in the β-barrel channel. Direct interactions between ion and backbone atoms do not occur, but they may occur between ion and channel side chain atoms, especially in those channels which have a hydrophilic lining. This observation has implications for ionic selectivity. The rough correlation with channel radius suggests that the reduction is to a large extent produced by confinement, but it is difficult in the present treatment to separate the effects of confinement on D from those caused by the presence of free energy barriers due to the strong electric field produced by the protein. Further work may be necessary to quantify and account for the effect of these free energy barriers, and perhaps to investigate ion–ion effects directly.

Acknowledgements

This work was supported by grants from the Wellcome Trust.

References

[1] J. Israelachvili, Intermolecular and Surface Forces, 2nd edn, Academic Press, New York, 1992.
[2] B. Hille, Ionic Channels of Excitable Membranes, 2nd. edn, Sinauer Associates Inc, Sunderland, MA, 1992.
[3] D.A. Doyle, J.M. Cabral, R.A. Pfuetzner, A. Kuo, J.M. Gulbis, S.L. Cohen, B.T. Chait, R. Mackinnon, Science 280 (1998) 69–77.
[4] G. Chang, R.H. Spencer, A.T. Lee, M.T. Barclay, D.C. Rees, Science 282 (1998) 2220–2226.
[5] D.W. Urry, Proc. Natl. Acad. Sci. USA 26 (1971) 672–676.
[6] B.A. Wallace, Biophys. J. 49 (1986) 295–306.
[7] L.K. Nicholson, Q. Teng, T.A. Cross, J. Mol. Biol. 218 (1991) 621–637.
[8] D.A. Doyle, B.A. Wallace, J. Mol. Biol. 266 (1997) 963–977.
[9] S.W. Cowan, T. Schirmer, G. Rummel, M. Steiert, R. Ghosh, R.A. Apuptit, J.N. Jansonius, J.P. Rosenbusch, Nature 358 (1992) 727–733.
[10] A. Kreusch, A. Neubueser, W. Schiltz, J. Wekesser, G.E. Schulz, Protein Science 3 (1994) 58–63.
[11] L. Song, M.R. Hobaugh, C. Shustak, S. Cheley, H. Bayley, J.E. Gouaux, Science 274 (1996) 1859–1866.
[12] N. Unwin, J. Mol. Biol. 229 (1993) 1101–1124.
[13] N. Unwin, Nature 373 (1995) 37–43.
[14] D.G. Levitt, Biophys. J. 59 (1991) 271–277.
[15] D. Chen, J. Lear, R.S. Eisenberg, Biophys. J. 72 (1997) 92–116.

[16] B. Roux, in: J.M. Goodfellow (Ed.), Modelling in Molecular Biology, VCH Verlagsgesellschaft, Weinheim, 1995, pp. 134–169.
[17] B.R. Brooks, R.E. Bruccoleri, B.D. Olafson, D.J. States, S. Swaminathan, M. Karplus, J. Comp. Chem. 4 (1983) 187–217.
[18] K. Cooper, E. Jakobsson, P. Wolynes, Prog. Biophys. Molec. Biol. 46 (1985) 51–96.
[19] S. Kuyucak, M. Hoyles, S.-H. Chung, Biophys. J. 74 (1998) 22–36.
[20] S-W. Chiu, J.A. Novotny, E. Jakobsson, Biophys. J. 64 (1993) 98–108.
[21] B.J. Berne, Multiple Time Scales, Academic Press, New York, 1985, pp. 419–436.
[22] B. Roux, Biophys. J. 74 (1998) 2744–2745.
[23] E. Jakobsson, S.-W. Chiu, Biophys. J. 52 (1987) 33–45.
[24] S.-W. Chiu, E. Jakobsson, Biophys. J. 55 (1989) 147–157.
[25] B. Roux, M. Karplus, Biophys. J. 59 (1991) 961–981.
[26] B. Roux, M. Karplus, J. Phys. Chem. 95 (1991) 4856–4868.
[27] B. Roux, M. Karplus, J. Am. Chem. Soc. 115 (1993) 3250–3262.
[28] G.R. Smith, M.S.P. Sansom, Biophys. J. 75 (1998) 2767–2782.
[29] S-W. Chiu, E. Jakobsson, S. Subramaniam, J.A. McCammon, Biophys. J. 60 (1991) 273–285.
[30] B. Roux, B. Prod'hom, M. Karplus, Biophys. J. 68 (1995) 876–892.
[31] R.M. Lynden-Bell, J.C. Rasaiah, J. Chem. Phys. 105 (1996) 9266–9280.
[32] M. Gutman, A. Tsfadia, A. Masad, E. Nachiel, Biochem. Biophys. Acta. 1109 (1992) 141–148.
[33] M. Sancho, M.B. Partenskii, V. Dorman, P.C. Jordan, Biophys. J. 68 (1995) 427–433.
[34] J. Breed, R. Sankararamakrishnan, I.D. Kerr, M.S.P. Sansom, Biophys. J. 70 (1996) 1643–1661.
[35] D.P. Tieleman, H.J.C. Berendsen, Biophys. J. 74 (1998) 2786–2801.
[36] M.E. Green, J. Lewis, Biophys. J. 59 (1991) 419–426.
[37] J. Green, J. Lu, Coll. Interface. Sci. 171 (1995) 117–126.
[38] M.S.P. Sansom, G.R. Smith, C. Adcock, P.C. Biggin, Biophys. J. 73 (1997).
[39] I.D. Kerr, R. Sankararamakrishnan, O.S. Smart, M.S.P. Sansom, Biophys. J. 67 (1994) 1501–1515.
[40] M.S.P. Sansom, R. Sankararamakrishnan, I.D. Kerr, Nature Struct. Biol. 2 (1995) 624–631.
[41] R. Sankararamakrishnan, C. Adcock, M.S.P. Sansom, Biophys. J. 71 (1996) 1659–1671.
[42] P.J. Kraulis, J. Appl. Cryst. 24 (1991) 946–950.
[43] O.S. Smart, J.M. Goodfellow, B.A. Wallace, Biophys. J. 65 (1993) 2455–2460.
[44] J.D. Lear, Z.R. Wasserman, W.F. DeGrado, Science 240 (1988) 1177–1181.
[45] J.D. Lear, Z.R. Wasserman, W.F. DeGrado. In Stephen H. White (Editor), Membrane protein structure, Oxford University Press, New York, 1994, pp. 335–354.
[46] P.K. Kienker, W.F. DeGrado, J.D. Lear, Proc. Natl. Acad. Sci. 91 (1994) 4859–4863.
[47] P.K. Kienker, J.D. Lear, Biophys. J. 68 (1995) 1347–1358.
[48] P. Mitton, M.S.P. Sansom, Eur. Biophys. J. 25 (1996) 139–150.
[49] Q. Zhong, Q. Jiang, P.B. Moore, D.M. Newns, M.L. Klein, Biophys. J. 74 (1998) 3–10.
[50] R.O. Fox, F.M. Richards, Nature 300 (1982) 325–330.
[51] G.A. Woolley, B.A. Wallace, J. Membr. Biol. 129 (1992) 109–136.
[52] M.S.P. Sansom, Quart. Rev. Biophys. 26 (1993) 365–421.
[53] D.S. Cafiso, Annu. Rev. Biophys. Biomol. Struct. 23 (1994) 141–165.
[54] S. You, S. Peng, L. Lien, J. Breed, M.S.P. Sansom, G.A. Woolley, Biochemistry 35 (1996) 6225–6232.
[55] G.A Wolley, P.C. Biggin, A. Scultz, L. Lien, D.C.J. Jaikaran, J. Breed, K. Crowhurst, M.S.P. Sansom, Biophys. J. 73 (1997) 770–778.
[56] J. Breed, P.C. Biggin, I.D. Kerr, O.S. Smart, M.S.P. Sansom, Biochim. Biophys. Acta 1325 (1997) 235–249.
[57] A. Karlin, M.H. Akabas, Neuron 15 (1995) 1231–1244.
[58] F. Hucho, V. Tsetlin, J. Machold, Eur. J. Biochem. 239 (1996) 539–557.
[59] F. Hucho, W. Oberthür, F. Lottspeich, FEBS Lett. 205 (1986) 137–142.
[60] A. Villarroel, S. Herlitze, M. Koenen, B. Sakmann, Proc. R. Soc. Lond. B 243 (1991) 69–74.
[61] B.N. Cohen, C. Labarca, L. Czyzyk, N. Davidson, H.A. Lester, J. Gen. Physiol. 99 (1992) 545–572.
[62] M.H. Akabas, D.A. Stauffer, M. Xu, A. Karlin, Science 258 (1992) 307–310.
[63] M.H. Akabas, C. Kaufmann, T.A. Cook, P. Archdeacon, J. Biol. Chem. 269 (1994) 14865–14868.
[64] F. Hucho, U. Görne-Tschelnokow, A. Strecker, Trends Biochem. Sci. 19 (1994) 383–387.
[65] D.L. Mielke, B.A. Wallace, J. Biol. Chem. 263 (1988) 3177–3182.
[66] J.-P. Changeux, J.I. Galzi, A. Devillers-Thiéry, D. Bertrand, Quart. Rev. Biophys. 25 (1992) 395–432.
[67] J.L. Galzi, A. Devillers-Thiéry, N. Hussy, S. Bertrand, J.-P. Changeux, D. Bertrand, Nature 359 (1992) 500–505.
[68] D. Bertrand, A. Devillers-Thiéry, F. Revah, J.L. Galzi, N. Hussy, C. Mulle, S. Bertrand, M. Ballivet, J.-P. Changeux, Proc. Natl. Acad. Sci. USA 89 (1992) 1261–1265.
[69] V. Gerzanich, R. Anand, J. Lindstrom, Mol. Pharmacol. 45 (1994) 212–220.
[70] G.R. Smith, M.S.P. Sansom, Biophys. J. 73 (1997) 1354–1381.
[71] F.A. Momany, R. Rone, J. Comp. Chem. 13 (1992) 888–900.
[72] S. Nosé, Molec. Phys. 53 (1984) 255–268.
[73] D.P. Tieleman, H.J.C. Berendsen, M.S.P. Sansom. Biophys. J., 76 (1999) 1757–1769.
[74] H.L. Grey, W.R. Schucany, The Generalized Jackknife Statistic, M. Dekker, New York, 1972.

[75] S. Koneshan, J.C. Rasaiah, R.M. Lynden-Bell, S.H. Lee, J. Phys. Chem. B 102 (1998) 4193–4202.
[76] B.J. Alder, T. Wainwright, Phys. Rev. A 1 (1970) 18–21.
[77] E.G.D. Cohen, Physica A. 194 (1993) 229–257.
[78] M.P. Allen, D.J. Tildesley, Computer Simulation of Liquids, Oxford University Press, Oxford, 1987.
[79] B. Roux, M. Karplus, Annu. Rev. Biophys. Biomol. Struct. 23 (1994) 731–761.
[80] M.O. Ortells, G.G. Lunt, Prot. Eng. 9 (1996) 51–59.
[81] D.B. Tikhonov, B.S. Zhorov, Biophys. J. 74 (1998) 242–255.
[82] C. Adcock, G.R. Smith, M.S.P. Sansom, Biophys. J. 75 (1998) 1211–1222.
[83] G.T. Ibragimova, R.C. Wade, Biophys. J. 74 (1998) 2906–2911.
[84] Y. Hao, M.R. Pear, D.D. Busath, Biophys. J. 73 (1997) 1699–1716.
[85] A. Skerra, J. Brickmann, Biophys. J. 51 (1987) 977–983.